Acceleration of premixed H2-Air-Steam flames when accounting for thermal radiation

Julie Ben Zenou, Ronan Vicquelin

Acceleration of premixed H_2-Air-Steam Flames when accounting for thermal radiation

J. Ben Zenou[a,*], R. Vicquelin[a]

[a]*Universite Paris-Saclay, CNRS, CentraleSupelec, Laboratoire EM2C, 8-9 rue Joliot Curie, Gif Sur Yvette, 91190, France*

Abstract

Diluting hydrogen flames with steam can increase flame stability and reduce nitrogen oxide emissions. While the effects of dilution on the flame characteristics due to variations in chemistry or transport properties have been well investigated, this is not the case for those related to thermal radiation. Thermal radiation is indeed often neglected in free flame simulations. However, it can be critical in diluted flames in which participating species are present in the fresh gases. This study explores thermal radiation's impact on H_2-Air flames diluted with steam through 1D laminar flame computations. To this end, a reactive fluid solver is coupled with a semi-analytical thermal radiation code. Both the grey gas approximation, for a preliminary understanding, and the more accurate CK narrow-band model, for detailed simulations that account for spectral-dependent gas properties, are used. The combustion numerical setup is validated against literature results. Three main thermal radiation effects are highlighted: a preheating of the fresh gases, an increased laminar flame speed, and a decreased temperature in the burnt gases. It is found that domain length considerably affects this preheating and flame speed, which can then affects laminar burning velocity measurements. It is shown that thermal radiation and combustion can often be decoupled and that a preheated adiabatic flame can recover the main characteristics of the corresponding radiative flame. The increase of the laminar flame speed by thermal radiation is reported for a wide range of equivalence ratios, dilution levels, and pressures. The observed acceleration is especially significant for lean and very lean flames which can be up to 500% faster when considering thermal radiation.

Keywords: Thermal radiation, Hydrogen Combustion, Laminar flame speed, Steam, Exhaust Gas Recirculation

Novelty and Significance Statement

This study provides a comprehensive investigation of the impact of thermal radiation on 1D laminar premixed H_2-Air flames diluted with steam, a topic not well-explored in the current literature. Using a reactive fluid solver coupled with a semi-analytical thermal radiation code, this research reveals significant effects of radiation on flame characteristics, including a preheating of the fresh gases and an increased laminar flame speed. The study emphasizes the importance of accurate gas radiative properties and domain length consideration. It demonstrates that thermal radiation can lead to an increase in flame speed of more than 50% for practical flames where $S_l \sim 20$ cm/s and even up to a 500% increase for very lean and diluted flames. These findings hold substantial implications for improving the accuracy of combustion modeling and offer valuable insights for the design and optimization of hydrogen combustion systems.

Author Contributions

JBZ performed the research. RV supervised the research.

1. Introduction

Hydrogen (H_2) combustion is considered in the medium term to neutralize the carbon emissions of several industrial processes and means of transport. However, hydrogen's fast chemical kinetics and high combustion temperature

*Corresponding author: julie.benzenou@gmail.com

lead to several difficulties, such as flame stabilization, flashback, or the emission of pollutants like nitrogen oxides (NOx).

One way to control the stability of this mixture and NOx emissions is to dilute the fresh gases with recirculated burnt gases, or steam. The study of H_2-Air-Steam mixtures is also essential in the context of nuclear safety. Indeed, a breach in the cooling system of a reactor leads to the presence of large quantities of steam which mixes with an explosive atmosphere containing mainly hydrogen and air [1].

The effect of steam dilution on flame characteristics has been studied for hydrogen (or syngas) flames both experimentally [1–7] and numerically [1, 4–9]. The main finding of these studies is that steam dilution reduces flame speed, adiabatic flame temperature, and NOx emissions. Three effects can explain this reduction: a thermal effect which is the most important one, a chemical effect summing a direct and third-body contribution, and a transport effect.

While it is known that thermal radiation emission by hot burnt gases affects the flame structure, temperature distribution, and pollutant production, the effects on the flame characteristics of radiation reabsorption by the fresh mixture are less understood and are generally neglected in free flame simulations. However, in these diluted flames, including thermal radiation (emission and reabsorption) in numerical simulations can be critical.

In the literature, two types of studies on the effect of thermal radiation in flames can be found: on one hand, some studies focus on spherical flames and mostly on the effect of the radiative heat loss in the burnt gases [9–13] while on the other hand, other articles study 1D planar flames and focus on the effect of radiation reabsorption by the fresh gases [14–18].

Studies from Zheng Chen and co-workers [9–13] study the effect of thermal radiation in spherical methane(CH4)-air flames diluted (or not) with carbon dioxide vapor (CO_2). They highlight the necessity to model radiation reabsorption as well as radiation emission to not overestimate the heat loss in the burnt gases. They find that considering thermal radiation, even with reabsorption, leads to a slight decrease in the laminar flame speed compared to adiabatic simulations. This is specific to spherical flames and the opposite effect is observed on diluted 1D planar flames.

Ju et al. [14] were among the first to study the effect of radiation reabsorption on 1D planar flames. They also focus on CH4/Air flames diluted with CO_2. They found that radiation reabsorption increases the flame speed and that the maximum flame temperature becomes higher than the adiabatic temperature. They also point out the important impact of the domain size on the results. Ruan et al. [15] completed this first study by insisting on the importance of an accurate radiation solver. They show that the optically thin or grey gas approximations are inadequate for such diluted flames. More recently, Shu Zheng and co-workers [16–18] also studied the importance of radiation reabsorption in 1D planar flames for example on ammonia flames [17] or on the combustion of biomass containing water [18].

Following these different studies, this work focuses on the effects of radiation reabsorption on 1D planar steam-diluted H_2 flames which, to these authors best knowledge, has not been considered yet. In addition, this manuscript adds a brick to the understanding of combustion/radiation coupling, in particular by highlighting the similarities between preheated adiabatic flames and coupled radiative flames. A systematic parametric study with variations of pressure, dilution ratio and equivalence ratio is also presented leading to the explanation of the role of every parameter on thermal radiation's strength. As dictated by the current literature, precise radiation models (non-grey and non-optically thin) are employed.

The main objectives of this manuscript are to (1) quantify the effect of thermal radiation on H_2-diluted laminar flame speeds for a large set of conditions (equivalence ratio, dilution level, pressure) and (2) identify the underlying physical mechanisms responsible for the observed effects.

To address these questions, the remainder of this article is organized as follows. The methods employed in the study are described in section 2. The results are then presented beginning with the validation of the numerical model in section 3. An in-depth analysis of the coupling for a single condition is presented in section 4, followed by a parametric study exploring the effects of various parameters (domain length, equivalence ratio, dilution level, pressure) in section 5. The conclusion and implications of the results are finally discussed in section 6.

2. Numerical Methods

2.1. Coupled fluid and radiative solvers

This work employs the in-house code Agath, developed at the EM2C laboratory, to solve the 1D steady Navier-Stokes equations for multi-species reactive flow. The 1D species transport equation for species k is written as :

$$\frac{\partial}{\partial t}\rho Y_k + \frac{\partial}{\partial x}\left(\rho\left(u + V_k\right)Y_k\right) = \dot{\omega}_k \tag{1}$$

where Y_k is the species mass fraction, ρ the mixture density, u the gas velocity, V_k the diffusion velocity and $\dot{\omega}_k$ the chemical source term. A similar transport equation is solved for enthalpy. In the considered steady state, the constant mass flux $\rho_u S_l$, with S_l the unstretched laminar flame speed and ρ_u the unburned gas density, is an eigenvalue value of the set of equations completed with boundary conditions. These equations are discretized with a finite volume scheme and solved with a Newton solver. Adaptative re-meshing is used to capture steep temperature and species fraction gradients in the flame front. The detailed mechanism by Varga et al. [19] is chosen for hydrogen combustion (12 species, 30 reactions), and a multicomponent formulation considering the Soret effect, as advised in [20], is used to model diffusion velocities.

This reactive flow solver is coupled to a 1D semi-analytical solver to describe radiative transfer in a heterogeneous slab domain. Starting from the integral formulation of the Radiative Transfer Equation (RTE), it is possible to obtain an exact expression in the 1D planar case. The local radiative power (P^R) can be broken down into two terms: an absorbed power (P^R_{abs}) and an emitted power (P^R_{em}). As found in Modest [21] (Eq. 14.34), those can be written as :

$$P^R(x) = P^R_{\text{abs}}(x) - P^R_{\text{em}}(x) \tag{2}$$

$$\begin{aligned}\text{with } P^R_{\text{abs}}(x) = &\int_0^\infty 2\pi\kappa_\nu(x)\left\{I^-_\nu(x_2)E_2[e_\nu(x,x_2)] + I^+_\nu(x_1)E_2[e_\nu(x_1,x)]\right\}d\nu \\ &+ \int_0^\infty d\nu \int_x^{x_2} 2\pi I^\circ_\nu(x')\kappa_\nu(x)\kappa_\nu(x')E_1[e_\nu(x,x')]dx' + \int_0^\infty d\nu \int_{x_1}^{x} 2\pi I^\circ_\nu(x')\kappa_\nu(x)\kappa_\nu(x')E_1[e_\nu(x',x)]dx'\end{aligned} \tag{3}$$

$$\text{and } P^R_{\text{em}}(x) = \int_0^\infty 4\pi\kappa_\nu(x)I^\circ_\nu(x)d\nu \tag{4}$$

where x_1 and x_2 are the bounds of the domain, ν is the wavenumber, $\kappa_\nu(x)$ is the local spectral absorption coefficient, $I^\circ_\nu(x)$ is the Planck black-body emission function at the temperature found at x, $I^+_\nu(x_1)$ and $I^-_\nu(x_2)$ are the two incoming radiative intensities from outside of the numerical domain, $e_\nu(x,x') = \int_x^{x'}\kappa_\nu(x'')dx''$ is the optical thickness of the slab between x and x' and $E_n(u) = \int_1^\infty e^{-ut}/t^n dt$ is the exponential integral of order n. These exponential integral functions are used here to express the slab transmissivities.

Two models for gas radiative properties are considered: a crude grey gas approximation and an accurate correlated-k (CK) model [22] with parameters updated by Rivière and Soufiani [23]. For the grey model, the value of κ is arbitrarily chosen. For the CK model, only H_2O is considered as a participating species. On each narrow-band, the integrals over the wavenumber are replaced by integrals between 0 and 1 using the inverse cumulative distribution function $k(g)$. More details can be found in section 11.9 in [21] or in [24]. These integrals are finally computed with Gaussian quadrature. The emitted power defined in Equation 4 is, for example, written as $P^R_{\text{em}}(x) = \sum_{i=1}^{N_{\text{band}}}\sum_{j=1}^{N_{\text{quadra}}} 4\pi k(g_{i,j})I^0_{\nu_i}\omega_{i,j}$ with $N_{\text{band}} = 44$ the number of narrow-bands, $N_{\text{quadra}} = 7$ the number of quadrature points in each narrow bands (see [23]) and where $g_{i,j}$ and $\omega_{i,j}$ are respectively the j-th quadrature points and weights in the i-th narrow band (in which $I^0_{\nu_i}$ is considered constant).

In this coupled setup, the fluid solver provides the temperature, pressure, and species fields to the radiative solver which, in turn, supplies the radiative power field, which is used as a source term in the Navier-Stokes energy equation.

For most simulations described in this paper, the domain goes from $x_1 = -L = -20$ cm to $x_2 = L = 20$ cm with the flame front located around 0 cm. Section 5.1 gives more insights into the domain length importance. The numerical results presented in the remainder of the paper are grid-independent (see Supplemental Material A for more details).

2.2. Boundary conditions

Each solver requires specific boundary conditions. For the fluid solver, a Dirichlet condition is imposed on the left side of the domain (fresh mixture), located far away from the flame front. A condition on the flux is used on the right side (burnt mixture). It is, for example, written as shown for the enthalpy :

$$(\rho u h_s)_N - (\rho u h_s)_{N-1} = \frac{1}{2}(\dot{\omega}_N + \dot{\omega}_{N-1})\Delta x_N + F^{\text{diff}}_{N-1} - F^{\text{diff}}_N \tag{5}$$

where h_s is the sensible enthalpy, N the number of points in the discretized domain, $\dot{\omega} = \dot{\omega}_T + P^R$ the source term, $\Delta x_i = x_i - x_{i-1}$ the mesh size and F^{diff} the diffusive flux. If the domain is large enough, the radiative power and chemical source term will be zero on the border and the diffusive flux will be constant. This equation then becomes a simple zero-gradient condition.

For the thermal radiation solver, the two incoming radiative intensities ($I^+_\nu(x_1)$ and $I^-_\nu(x_2)$) must be prescribed. Any radiative heat transfer within the gas outside of the numerical domain is neglected. It is assumed that the gas is surrounded by a cold black enclosure. This leads to $I^+_\nu(x_1) = I^-_\nu(x_2) = I^0_\nu(T_w)$ where $T_w = 500$ K is the prescribed enclosure temperature.

2.3. Conditions studied

Mixtures of hydrogen, air and steam are considered in this study. The inlet unburned gas temperature is set to 500 K for all conditions. This high temperature is chosen for two reasons: it is representative of actual engine conditions [25–29], and it is higher than water ebullition temperature at 20 atm (483.15 K). This means that water will only exist as steam and not as a liquid in the simulations of this paper. Equivalence ratios, ϕ, between 0.3 and 2, dilution levels, denoted by the steam mass fraction in the fresh gases $y^0_{H_2O}$ between 0 and 40% and pressures, p between 1 and 20 atm are studied here. When steam is added to the mixture for dilution, the ratios $y^0_{H_2}/y^0_{O_2}$ and $y^0_{N_2}/y^0_{O_2}$ are kept constant. An undiluted mixture of H_2 and Air at a given equivalent ratio is first created and then mixed with steam. In the final diluted mixture, the mass fraction of hydrogen, for example, can thus be written as $y^0_{H_2} = (1 - y^0_{H_2O})y^{\text{undiluted}}_{H_2}$. For each set of conditions, an adiabatic flame, i.e., without thermal radiation, and the corresponding coupled radiative flame are simulated. This means that water will only exist as steam and not as a liquid in the simulations of this paper. Equivalence ratios, ϕ, between 0.3 and 2, dilution levels, denoted by the steam mass fraction in the fresh gases $y^0_{H_2O}$ between 0 and 40% and pressures, p between 1 and 20 atm are studied here. For each set of conditions, an adiabatic flame, *i.e.*, without thermal radiation, and the corresponding coupled radiative flame are simulated.

3. Validation

Before studying the thermal radiation effects on diluted flames, this section's objective is to make sure that the combustion modeling setup is accurate to determine H_2-Air laminar burning velocities. To this end, numerical results of adiabatic simulations of undiluted and diluted H_2 flames are compared to experimental values found in the literature. A validation of the implementation of physical models in our solvers is presented in Supplemental Material A by comparison with other numerical results (obtained with Chemkin PREMIX [30] for combustion or a Line-By-Line description of the radiative properties for thermal radiation).

3.1. Validation for different equivalence ratios

Several authors [31–42] reported experimental values of the laminar flame speed for non-diluted H_2-Air mixtures at normal conditions of temperature and pressure. In these non-diluted flames, thermal radiation's impact on the laminar flame speed is negligible and adiabatic simulations can be compared to experiments. The results of this comparison for the adiabatic flame speed, S_l, are aggregated in Figure 1. The numerical results are obtained with the Varga [19] mechanism and a multicomponent transport description. The results are plotted with and without the Soret effect to show the impact of thermal diffusion on H_2 flames. This figure validates the kinetic scheme and transport description used in this work for adiabatic simulations without dilution at normal conditions of temperature and pressure.

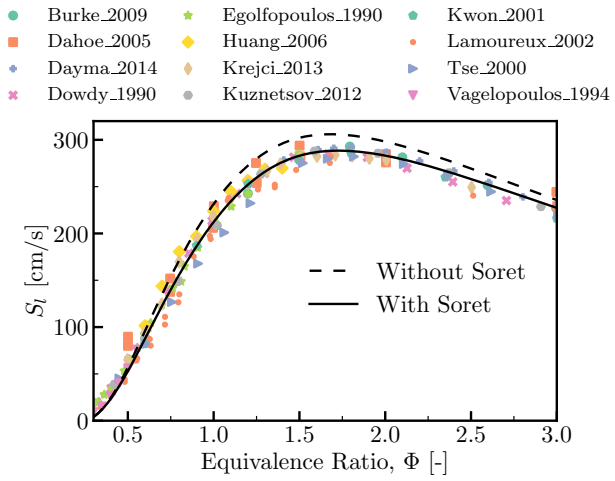

Figure 1: **Validation of cinetic scheme and transport description.** Laminar flame speed of adiabatic H_2-Air flames at T_u = 300 K and p = 1 atm for varying equivalence ratio. Colored symbols are experimental results [31–42] and lines are numerical results with the Varga [19] kinetic scheme and a multicomponent description with or without the Soret effect.

3.2. Validation for different pressures and temperatures

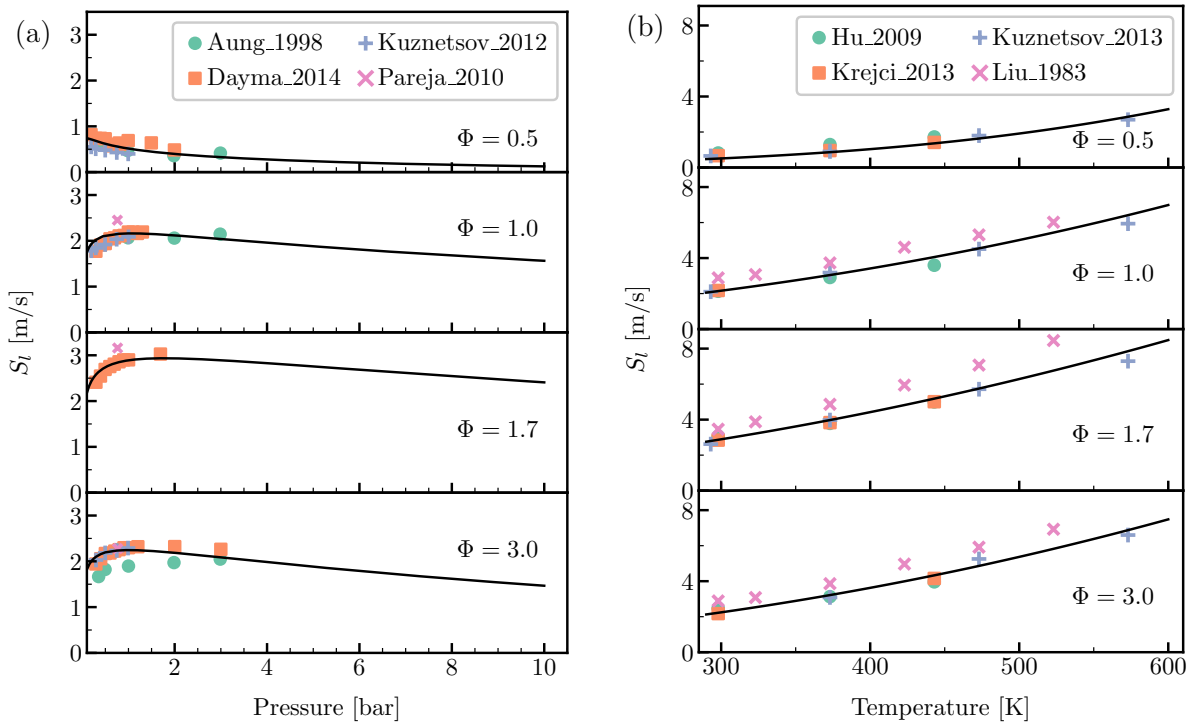

Figure 2: **Validation for different pressure** (a) **and temperature** (b) **conditions.** Laminar flame speeds of adiabatic H_2-Air flames at T_u = 300 K (a) or p = 1 atm (b) and four different equivalence ratios for a varying pressure (a) or temperature (b). Lines are numerical results and colored symbols are experimental results [2, 33, 37, 38, 43–46].

Experimental values of the laminar flame speed for non-normal pressures and temperatures are more sparse. This is especially true for high-pressure values where instabilities appear in spherical flames. Some experimental results for a varying pressure are presented in Figure 2a at four different equivalence ratios and for $T_u = 300$ K [33, 38, 43, 44]. They are compared to results from adiabatic simulations. Except at $\phi = 3$, the numerical results for a varying pressure agree well with the experimental ones. At $\phi = 3$, numerical results are consistent with the flame speeds from Dayma et al. [33] but the values from Aung et al. [43] are significantly lower. It is known that, for rich mixtures, this study from 1998 gives consistently lower values of flame speeds than other experimental studies [47]. The discrepancies between the simulations' results and those from Aung et al. are thus not very concerning.

Figure 2b presents the same comparison but for a varying temperature at $p = 1$ atm. The experimental data are taken from [2, 37, 45, 46]. With a varying temperature, numerical results are close to most experimental values except the ones from Liu et al. [2]. The flame speeds of this study were obtained with a burner method, considered less accurate today. This could explain the observed differences.

Overall, these results validate the chemical kinetics scheme and transport description used in this work for different pressures and temperatures for non-diluted adiabatic H_2-Air flames.

3.3. Validation for different dilution levels

Some studies also give experimental values of the unstretched laminar flame speed for H_2-Air flames diluted with steam. They all consider a preheated fresh mixture to cover a wide range of steam content while avoiding condensation. The fresh gases temperature vary between 323 K for [4], 363 K for [1], 353 for [48] and 373 K for [2, 3, 7]. In these diluted flames, the effect of reabsorption on the flame speed can be substantial. Thus these experimental results are compared in Figure 3 with adiabatic and radiative numerical results at $p = 1$ atm. The differences between adiabatic and radiative results will be more detailed in the following two sections but it appears they are more important for leaner flames ($\phi = 0.45$ in Figure 3a) and more diluted flames ($x_{H_2O} = 0.3$ in Figure 3b).

It is first necessary to highlight that the y-axis range of the first subplot of Figure 3a corresponding to $\phi = 0.45$ is about ten times smaller than that of the other subplots of this figure. Numerical radiative results at $\phi = 0.45$ are close to experimental one from Lamoureux et al [48] (difference of about 5% at the maximum dilution level studied). The difference between the experimental values and the numerical adiabatic ones is more important. This difference seems to increase with increasing dilution levels. Accounting for radiation bridges the gap between the two curves, but this result should be treated cautiously. The experimental results from Das *et al.* [4] present the same tendencies but have lower absolute values because the preheating temperature of the experiments is only 323 K compared to the 363 K of the simulations.

The numerical results for the other equivalence ratios presented in Figure 3a agree with the most recent experimental ones from Grosseuvres et al. [1]. The results from Liu et al., Koroll et al. and Lyu et al. [2, 3, 7] were obtained with the burner method, which, as detailed earlier, can be less precise and more impacted by stretch effects.

Figure 3b presents the same kind of results but for a varying equivalence ratio at three fixed dilution levels. This makes it easier to see the differences for rich diluted flames that are not very visible in Figure 3a due to scale effects. For most conditions, it appears that coupled radiative results are closer to experimental ones but still a bit lower.

As will be more detailed in Section 5.1, the comparison of the 1D planar coupled numerical results with experimental results is made difficult by the differences in geometry and domain size considered. Indeed, experiments are based on counterflow or spherical flames in which thermal radiation effects are very different from those observed in a 1D planar flame (see [10] for example).

Overall, the trends observed experimentally are well-matched numerically. More work is necessary to quantitatively validate these results, especially when thermal radiation is involved. The remainder of this manuscript focuses exclusively on analyzing the effects of thermal radiation.

4. In-depth analysis of the coupling with thermal radiation for a single condition

In this section, a single condition is thoroughly studied. The chosen flame is a H_2-Air-Steam flame at $p = 5$ atm, $\phi = 0.8$, $y^0_{H_2O} = 0.3$. The fresh gas temperature is always $T_u = 500$ K. The adiabatic laminar flame speed of this flame is 22 cm/s. First, a grey gas approximation is used to model gas radiative properties in order to better understand the coupling between combustion and thermal radiation. This simple model is then replaced with more detailed radiative properties using a CK model.

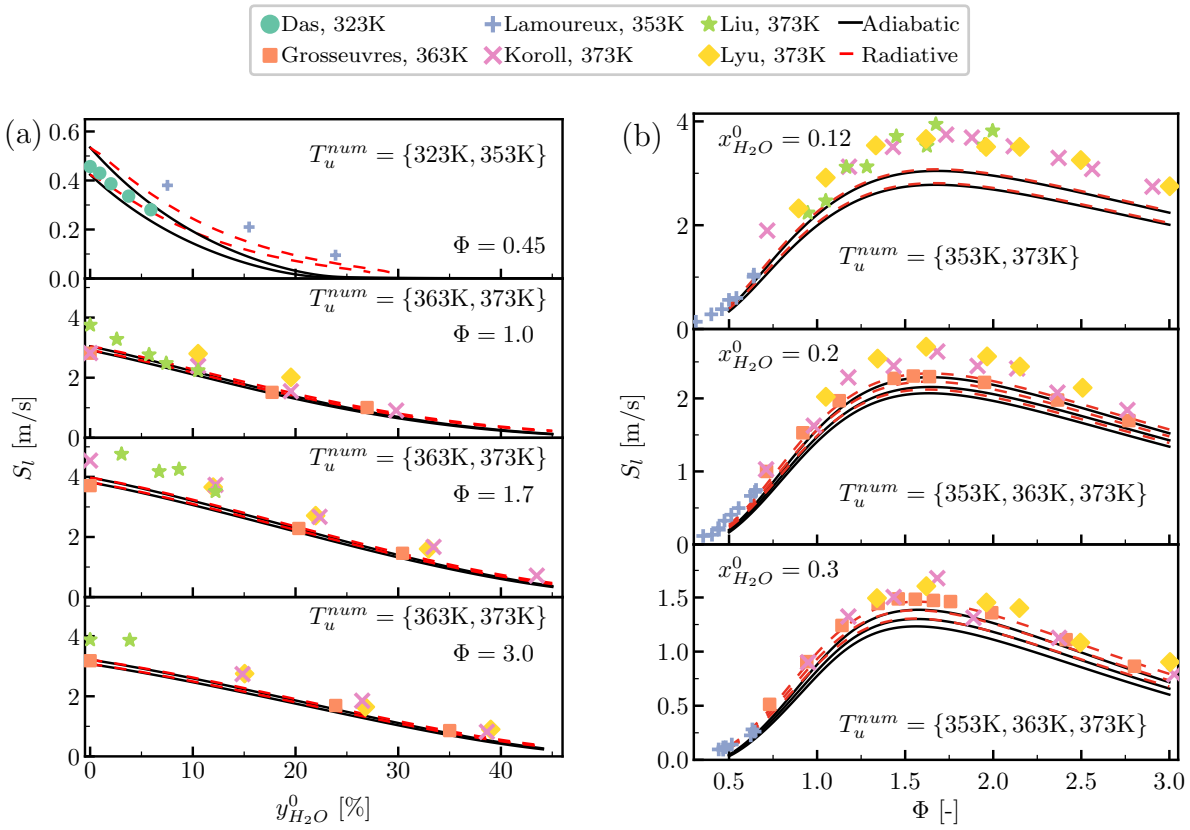

Figure 3: **Validation for different dilution levels.** Laminar flame speed of H_2-Air flames at $p = 1$ atm. (a) : four equivalence ratios for varying dilution levels. (b) : three dilution levels for varying equivalence ratios. Colored symbols are experimental results [1–4, 7, 48]. The fresh gases temperature is reminded in the legend for each experimental dataset. For accurate comparisons, the initial temperatures of the numerical simulations match the experimental conditions. The adiabatic simulations are plotted in solid black lines. The radiative coupled calculations, which use a CK model, are plotted in red dashed lines. For the radiative simulations, the enclosed temperature is the same as the fresh gases temperature. The progression from lower to higher flame speed curves mirrors the progression from lower to higher initial temperatures in each subplot, allowing the identification of each numerical case.

4.1. Grey Gas

Three different values of uniform absorption coefficients, κ, are considered: $\kappa = 0.1$ m^{-1}, $\kappa = 1$ m^{-1}, and $\kappa = 10$ m^{-1}. With $L = 20$ cm, these lead to optical thicknesses, κL, of 0.02, 0.2, and 2. Those values correspond to transmissivities of the fresh or burnt gas slab, $\tau = \exp(-\kappa L)$, of 0.98, 0.82, and 0.14. These values are chosen arbitrarily since the objective of this section is not to obtain accurate results or quantify the inaccuracy of the grey model but rather to understand the key parameters and phenomena at stake in the coupling between combustion and thermal radiation. The flames' temperature and radiative power profiles corresponding to each value of κ are plotted in Figure 4. The corresponding adiabatic (*i.e.* without thermal radiation or $\kappa L = 0$ and $\tau = 1$) temperature profile is also compared.

For all values of κL, the radiative power is negative in the hot gases where emission is dominant and positive in the unburned gases, which mainly absorb thermal radiation. In the burnt gases, this emission leads to a decrease in the temperature. Part of this emission is reabsorbed by steam in the fresh gases. This leads to a preheating of the mixture before the flame front. This preheating is stronger for higher values of κ since a higher absorption coefficient means more emission from the hot gases (for a fixed temperature), and a greater optical thickness means more reabsorption from the fresh gases as well as a minimized impact of the cold boundaries on the rest of the domain.

The fresh gases cannot reabsorb all the emitted thermal radiation; some is lost at the cold boundaries. These losses

are highlighted by the temperature value at the last point of the simulated domain, which is lower than the adiabatic flame temperature of 1650 K for all κL.

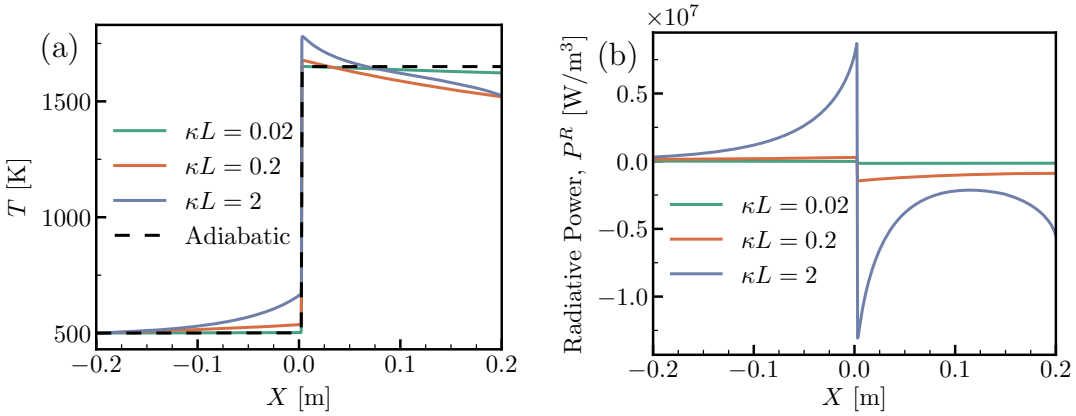

Figure 4: **Temperature** (a) **and radiative power** (b) **profiles with the grey-gas approximation**. Three grey optical thicknesses are considered at p = 5 atm, ϕ = 0.8 and $y^0_{H_2O}$ = 0.3. The dashed line corresponds to the adiabatic temperature profile.

The preheating of the fresh gases has two main consequences: the maximum temperature in the domain is higher than the adiabatic flame temperature, and the unstretched laminar flame speed is increased. The flame speeds for the different κL are summarized in Table 1 together with the corresponding relative difference $R = (S_l^{\text{rad}} - S_l^{\text{adiab}})/S_l^{\text{adiab}}$. This coefficient, similar to the one defined in [12], quantifies the effect of thermal radiation on the flame speed. In the optically thin case (κL = 0.02), the value of the flame speed is very close to the adiabatic one, which translates by a small value of R = 1%. For higher values of κL, the acceleration (in this manuscript, "acceleration" is used to refer to an increase in the laminar flame speed) due to thermal radiation is more important, and R reaches 170% for κL = 2.

Table 1: Laminar flame speeds for different optical thicknesses κL with the grey-gas approximation.

Radiation Model	κL [-]	S_l [cm/s]	R [%]
Adiabatic	0	22.0	0
Grey Gas	0.02	22.3	1
	0.2	27.8	26
	2	59.4	170

Increasing κ from 0.1 to 10 m^{-1} in a 40 cm domain gives the same optical thickness as keeping κ = 0.1 m^{-1} constant but increasing the domain length from 40 cm to 40 m. This suggests that domain length can significantly impact thermal radiation's strength. This was shown in [14] and will be more detailed in section 5.1.

4.2. Spectral-dependent radiative gas properties

A low-resolution emissivity spectrum of the burnt gases obtained with the CK Model detailed in section 2.1 is presented in Figure 5. The scaled Planck black-body emission function at the adiabatic flame temperature T_{adiab} = 1650 K is also displayed to highlight the area of interest in the spectrum. It appears clearly that the studied mixture is not grey.

To situate the CK flame in comparison to the grey flames described before, it may be interesting to define a mean transmissivity of the burnt gases weighted by the Planck function: $\overline{\tau} = \int_0^\infty \kappa_\nu I^0_\nu d\nu / \int_0^\infty I^0_\nu d\nu$ = 0.72. The domain is therefore neither optically thin nor optically thick. Figure 6 compares the CK model simulation with the adiabatic results. The effects of thermal radiation on this coupled flame are qualitatively the same as those observed with the grey gas approximation in the previous section: a preheating of the fresh gases, a maximal temperature higher than the

adiabatic temperature, a decrease in the burnt gases temperature and an acceleration of the flame. This acceleration is significant with a radiative flame speed S_l^{rad} of 34 cm/s corresponding to a R factor of 55%. It is worthwhile to note that these qualitative effects are similar to those observed in porous burners where the heat recirculation from hot gases to the fresh gases happens inside the solid structure instead of thanks to thermal radiation [49].

To accurately quantify the acceleration of diluted flames due to thermal radiation, careful consideration of spectral-dependent radiative properties is necessary. While employing more detailed models, such as the CK model chosen in this study, increases the computational cost (requiring hundreds of radiative transfer equation resolutions instead of a single one with the grey gas approximation), it is important to note that using a simple grey gas model is notoriously inappropriate. Global models such as the weighted-sum-of-gray-gases model (WSGG, [50, 51]) or the Spectral Line WSGG model (SLW, [52]) are not considered here to focus on accuracy and high-fidelity results provided by the CK narrow-band model, in line with the reciprocal detailed combustion modeling setup.

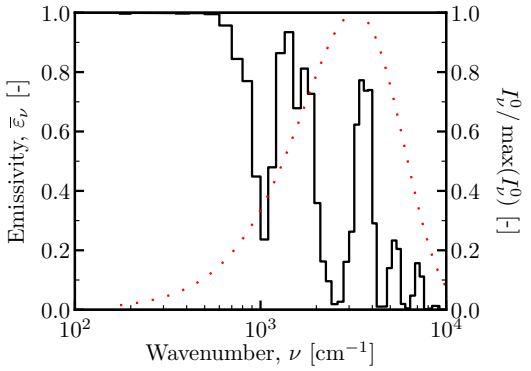

Figure 5: **CK Emissivity spectrum** of the burnt mixture of a $\phi = 0.8$, $y^0_{H_2O} = 0.3$, $p = 5$ atm flame. The dotted red line corresponds to the scaled Planck black-body emission function at $T_{\text{adiab}} = 1650$ K.

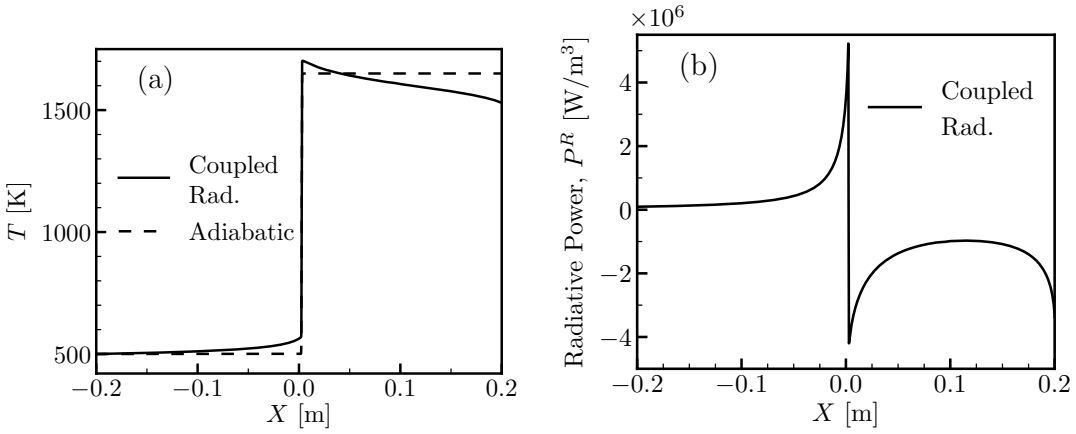

Figure 6: **Temperature** (a) **and radiative power** (b) **profiles obtained with the CK model**. $p = 5$ atm, $\phi = 0.8$ and $y^0_{H_2O} = 0.3$. The adiabatic temperature profile is plotted in dashes for comparison.

Thermal radiation also affects the flame structure. Figure 7 shows some minority species profiles (H and OH radicals) as a function of the steam mass fraction in the domain. This phase diagram allows for a zoom on the flame front. The impact of thermal radiation on these intermediate radical species is significant with an increase of the

maximum value of y_H of 67%, for example.

To reiterate, it has been shown that in a realist configuration with a detailed spectral-dependent model, a detailed chemical mechanism, and accurate transport modeling, taking thermal radiation into account leads to an increase in the laminar flame speed of 55%. Thus, in this H_2-Air-Steam flame at $\phi = 0.8$, $y^0_{H_2O} = 0.3$, $p = 5$ atm and $T_u = 500$ K, it is essential to consider thermal radiation to achieve a correct simulation of the flame velocity.

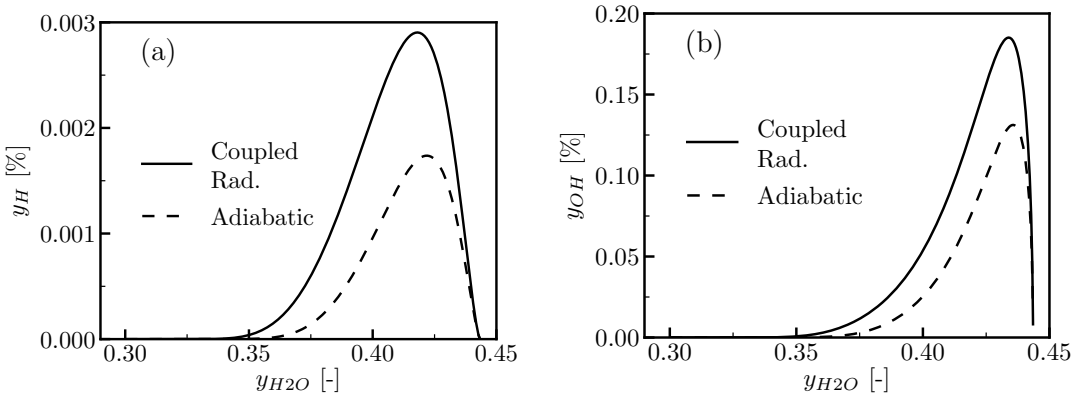

Figure 7: **Minor species profiles as a function of steam mass fraction** y_H (a) and y_{OH} (b) profiles obtained with the CK model. The x-axis is y_{H_2O} to zoom inside the flame front. $p = 5$ atm, $\phi = 0.8$ and $y^0_{H_2O} = 0.3$. The adiabatic profiles are plotted in dashes for comparison.

4.3. Equivalent adiabatic preheated flame

The acceleration due to thermal radiation seems to be caused by the fresh gases' preheating. This section wants to prove that this is, indeed, the main cause for the increase in S_l. To this end, it is first interesting to compare the characteristic scales of thermal radiation, convection and combustion.

The radiative time scale,τ^{rad} is written as detailed in [53]:

$$\tau^{\text{rad}} = \frac{c_p/r}{P^R_{\text{abs}}/p} \tag{6}$$

where P^R_{abs} is, as defined in section 2.1, the local absorbed power in the fresh gases and r is the specific gas constant of the fresh mixture. For a quick estimate of the radiative time, Binauld et al [53] suggest evaluating the power absorbed locally by assuming an infinitely thin layer of fresh gases and an homogeneous slab of burnt gases. The absorbed power in the fresh gases can then be easily estimated. For the considered flame, with 30% H_2O in the fresh gases (which leads to 44% of H_2O in the burnt gases), $T_u = 500$ K, $T_{\text{adiab}} = 1650$ K, $p = 5$ atm and $L = 20$ cm, the computation leads to $\tau^{\text{rad}} \sim 0.3$ s.

This characteristic time can be compared to a convective time in the fresh gases written as $\tau^{\text{conv}} = L/S_l \sim 0.6$ s. Since τ^{rad} is smaller than τ^{conv}, a strong preheating of the fresh gases is expected.

On the other hand, the radiative time can also be compared to a chemical time scale. This combustion characteristic time can be written using the flame thickness and the flame speed as $\tau^{\text{chem}} = \delta_l/S_l$. This flame thickness is obtained through a tangent method as $\delta_l = (y^{\max}_{H_2O} - y^{\min}_{H_2O})/\max(dy_{H_2O})$. For the considered flame, the simulation gives $\delta_l \sim 0.2$ mm and $\tau^{\text{chem}} \sim 0.5$ ms. Thus, $\tau^{\text{chem}} \ll \tau^{\text{rad}}$. This difference in time scales indicates that thermal radiation and combustion can be partially decoupled. This decoupling implies that radiation effects within the flame front itself are negligible. Thermal radiation will only affect fresh gases before the flame front and burned gases downstream. We discuss these two points. Firstly, although the radiative losses on the burned gases side undoubtedly affect the downstream temperature profile post-flame, they cannot significantly propagate back into the flame front or modify the fresh gases behavior in such 1D flames. Note that this differs in spherical flames, where a hydrodynamic effect would modify the fresh gases acceleration. Thus, the influence of heat losses in the burned gases on the flame's velocity or structure remains minimal in this study's context. Secondly, the preheating of fresh gases due to their reabsorption

of thermal radiation occurs before the flame front, modifying its response. Still, the physical mechanisms within the flame itself are left undisturbed.

To prove this decoupling of thermal radiation and combustion, an adiabatic preheated flame is compared to the coupled radiative solution. First, the preheating temperature is found at the first point in the numerical domain (x_{preheat}) where $(y_{H_2O} - y^0_{H_2O})/(y^{+\infty}_{H_2O} - y^0_{H_2O}) > 0.1\%$. In this expression, $y^0_{H_2O}$ is the mass fraction of steam in the fresh gases while $y^{+\infty}_{H_2O}$ is the mass fraction of steam downstream of the flame. This gives $T_{\text{preheat}} = 568$ K for the considered flame with $\phi = 0.8$, $y^0_{H_2O} = 0.3$ and $p = 5$ atm. An energy balance between $x_1 = -L$ and x_{preheat}, assuming a constant c_p in the fresh gases, leads to :

$$T_{\text{preheat}} = T_u + \frac{Q^{\text{rad}}}{\rho_u S_l c_p} \tag{7}$$

where Q^{rad} is the integrated radiative power between x_1 and x_{preheat}. The coupled simulation gives $Q^{\text{rad}} = 90$ kW/m^2, $\rho_u S_l = 0.86$ kg/m^2/s and $c_p \sim 1530$ J/K/kg. Equation 7 with these values results in the same value of preheating, *i.e* $T_{\text{preheat}} = 568$K. This energy balance confirms that only thermal radiation is responsible for the observed preheating in the fresh gases.

An adiabatic simulation with the same composition as before but with $T_u = T_{\text{preheat}}$ instead of $T_u = 500$ K is run. The results are compared with the coupled flame with the CK model in Figure 8. As seen in Figure 8a, the maximal temperature of the radiative flame is well recovered by the preheated adiabatic flame. The mass flux $\rho_u S_l$ is also really close with a value of 0.847 kg/m^2/s for the adiabatic preheated flame compared to 0.855 kg/m^2/s for the radiative flame. As reference, the adiabatic value found with $T_u = 500$ K was 0.56 kg/m^2/s.

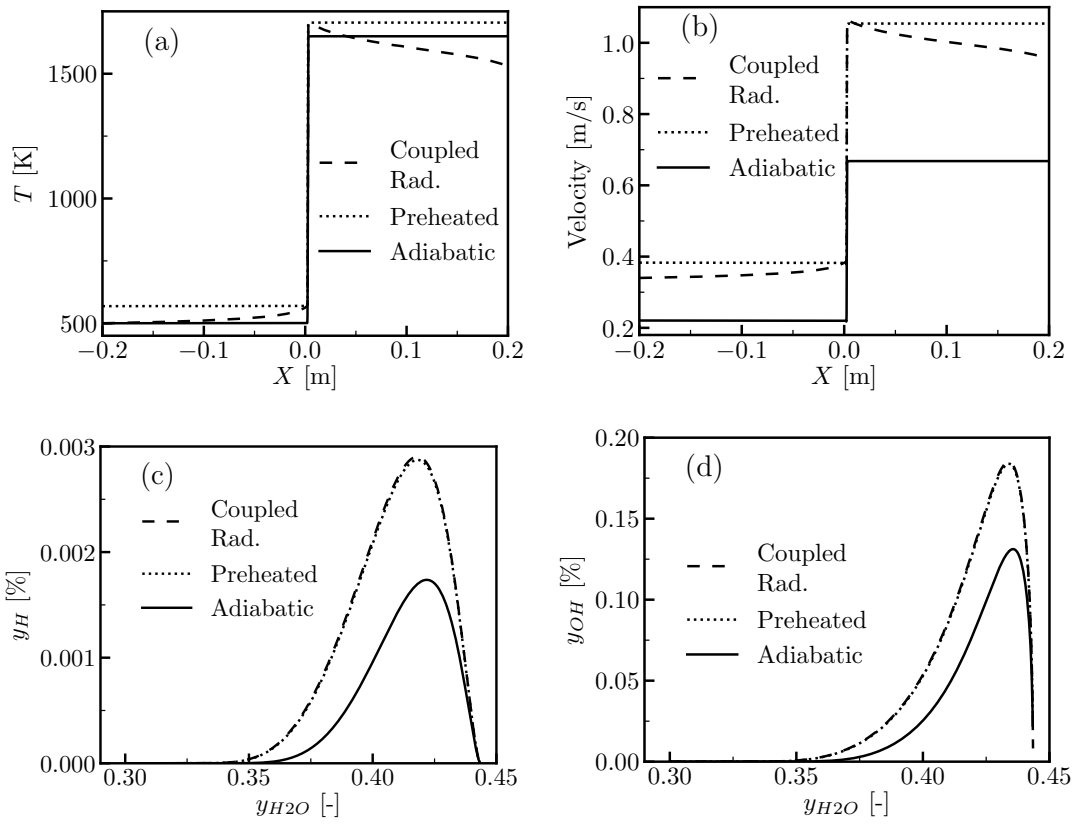

Figure 8: **Comparison of the temperature** (a) **, the velocity** (b) **and the H** (c) **and OH mass fractions** (d) **profiles of the adiabatic preheated and the radiative flames.** $p = 5$ atm, $y^0_{H_2O} = 0.3$ et $\phi = 0.8$. For the radiative flame, the CK model is used and $T_u = 500$K. For the preheated flame $T_u = T_{\text{preheat}} = 568$K. The initial adiabatic flame's profiles with $T_u = 500$K are also plotted for comparison.

Figure 8b shows that the velocity in adiabatic flames is constant in the fresh and burnt gases. This is not true for the coupled radiative simulation in which mass conservation and temperature variation impose an increasing velocity in the fresh gases. Thus, to compare the radiative and preheated flame speeds (which are the flames' velocities at the first point of the numerical domain), a correction due to the different densities must be applied. Indeed, the equality of the burning mass flow rates can be written as $(\rho_u S_l)^{\text{preheat}} = (\rho_u S_l)^{\text{rad}}$. Using the ideal gas law to connect density and temperature, it follows that $\widehat{S_l}^{\text{rad}} = 500\text{K}/T_{\text{preheat}} * S_l^{\text{preheat}}$ where $\widehat{S_l}^{\text{rad}}$ is the estimated value of the radiative flame speed from the adiabatic preheated result, S_l^{preheat}. Applied to the considered flame, where $S_l^{\text{preheat}} = 38.2$ cm/s, it leads to $\widehat{S_l}^{\text{rad}} = 33.6$ cm/s which is remarkably close to the simulated value of $S_l^{\text{rad}} = 34$ cm/s.

Figures 8c and 8d show that the radiative flame structure, characterized by y_H and y_{OH} profiles, is also well recovered by the adiabatic preheated flame.

Overall, it has been shown that, first, knowing the integrated radiative power in the fresh gases, the preheating can be easily computed by an energy balance. Once this preheating is known, it is possible to recover the radiative flame speed or inner structure with an adiabatic preheated flame. However, it should be emphasized that this methodology does not account for radiative losses in the burned gases. As a result, the temperature profile after the flame front predicted by the adiabatic preheated flame differs from the radiative one. Nonetheless, given the previously discussed characteristic time scales and insights from prior research on non-diluted flames, such as that of [14], the temperature drop in the burnt gases has no significant effects on the flame's velocity or its intrinsic structure.

5. Parametric Study

In the previous section, the effect of thermal radiation on diluted H_2-Air flame has been investigated for one condition. This section studies what happens when several parameters such as the domain length, the equivalence ratio, the dilution level or the pressure are varied.

5.1. Domain length

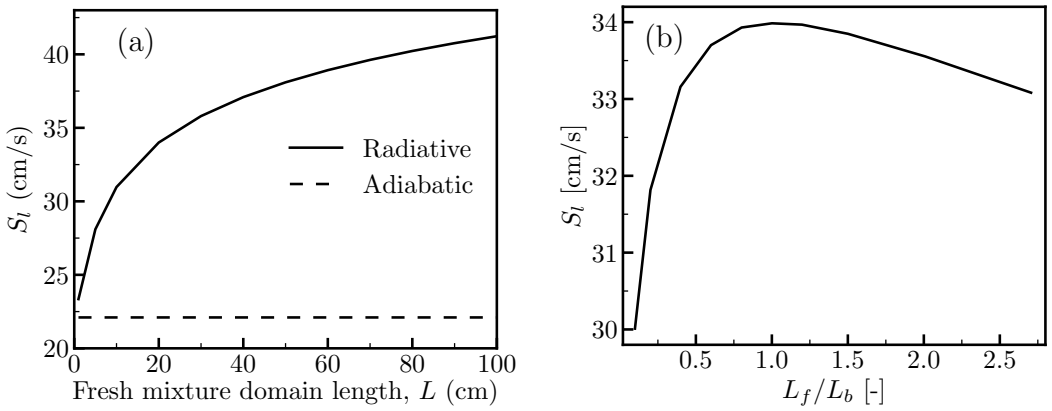

Figure 9: **Impact of the total domain length (a) and the ratio L_f/L_b (b), with L_f and L_b the length of the fresh and burnt gases slabs, on the flame speed in a radiative coupled simulation with the CK model.** $T_u = 500$K, $p = 5$ atm, $y^0_{H_2O} = 0.3$ et $\phi = 0.8$. The adiabatic flame speed, which does not depend on L, is plotted in dashes in (a) for comparison. In (b), the total domain length is constant and equal to 0.4m.

It has been suggested in 4.1 that domain length could significantly impact the acceleration due to thermal radiation. To quantify this impact on a coupled simulation with the CK model, several flames, with $\phi = 0.8$, $y^0_{H_2O} = 0.3$, $p = 5$ atm and $T_u = 500$ K, were calculated in increasing domains between 2 cm and 2 m. The variation of the flame speed as a function of the fresh gases' slab thickness, L, is presented in Figure 9. For each simulation, the total domain length is $2L$. As expected, the radiation effect drops for small values of L but does not disappear either. Even for large

domains with $L \sim 1$ m, the effect of thermal radiation keeps increasing significantly when the domain gets larger. This suggests that a converged solution would require a non-realistic domain length. Quantitatively speaking, the flame speed increases from 23.3 cm/s for $L = 1$ cm to 41.2 cm/s for $L = 1$ m. This represents a R factor (defined in section 4.1) of respectively 6% and 87%. The effect of domain length on the flame acceleration is thus consequent. In practical combustion applications, where the chamber dimensions range from tens of centimeters up to several meters, a finite configuration with the proper length must thus be simulated to obtain the accurate radiative flame speed. This influence of domain length on the laminar flame speed explains why it is particularly hard to compare these coupled numerical results to experimental ones.

Moreover, as presented in section 3, most experimental flame speeds are obtained through spherically expanding experiments. In this geometrical configuration, the ratio of fresh and burnt gases thicknesses L_f and L_b is not one anymore. Figure 9b depicts the influence of this ratio on the flame speed of coupled radiative flames. It can be seen that the effect of thermal radiation is maximum when the ratio is close to one, which corresponds to the flames studied in this manuscript. In spherically expanding flames, L_f/L_b is generally much higher than 1 [54] so the effect of thermal radiation is not as important. In addition to this effect due to the L_f/L_b ratio, one must also consider the specificities of the radiative transfer equation in spherical flames, which does not have the same solution as in a planar geometry. For these reasons, it is very difficult to compare the 1D planar numerical results with those obtained experimentally on spherical flames (see Chen et al. [9–12, 55] for example).

Thermal radiation effect thus depends on domain length and, more generally, on the geometry. The advantage of planar simulations, studied here numerically, is that they directly give the unstretched laminar flame speed without any extrapolation contrary to spherical flames. They are however harder to compare to experimental results.

5.2. Equivalence ratio and dilution level

Varying the equivalence ratio of a flame impacts its flame speed. According to Eq. 7, this means that a change in equivalence ratio is going to influence the preheating of the fresh gases and as such, is going to affect the acceleration of the flame due to thermal radiation. On the other hand, varying the dilution level means changing the mass fraction of H_2O in the fresh and burnt gases as well as the burnt mixture's temperature. This leads to variations in S_l and Q^{rad} which, still according to Eq. 7, impacts the preheating. Thus, the effect of thermal radiation on diluted flames depends on the equivalence ratio and the dilution level of the considered flame.

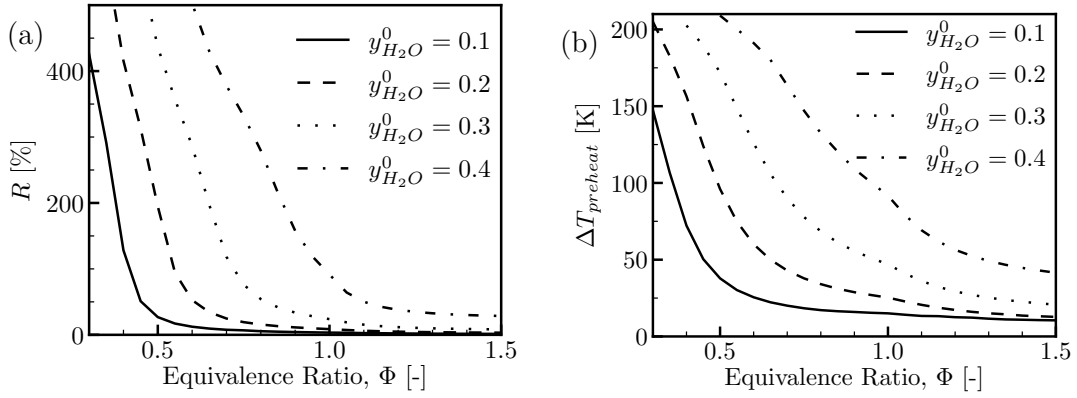

Figure 10: **Impact of equivalence ratio and dilution level on the relative flame speed change** R (a) **and on the preheating** (b) for $p = 5$ atm, $T_u = 500$K and $L = 20$ cm. The coupled radiative simulations are carried out with a CK model.

Figure 10a illustrates the effect of thermal radiation on the laminar flame speed, quantified by the R factor, as a function of equivalence ratio, for $p = 5$ atm and different values of dilution level between 10% and 40%. The various simulations carried out to obtain this figure, and all others in this section, were done with a 40 cm long domain ($L = 20$ cm). The coupled radiative simulations were carried out with the same CK model detailed and used previously. First, as expected, higher dilution results in a more significant impact of thermal radiation. Indeed, the main effect of a higher dilution level is a reduced flame speed, as observed in Figure 3 in section 3. As seen in Eq. 7, this leads to

more preheating of the fresh gases. Moreover, increasing the dilution level means more steam in the fresh and burnt gases but colder burnt gases. This can lead to smaller or higher values of Q^{rad} depending on the conditions. This effect (not shown) on Q^{rad} is, in any case, small compared to the effect on the flame speed. This decrease in flame speed results in an overall increase in the preheating that can be observed in Figure 10b where $\Delta T_{\text{preheat}} = T_{\text{preheat}} - 500\text{K}$ is plotted as a function of equivalence ratio for different dilution levels. Finally, this greater preheating ends up leading to a greater acceleration.

It also appears that leaner flames, especially those with $\phi < 0.5$ are much more impacted by radiation. There are two reasons for this. First, lean flames are the slowest. As detailed earlier, Eq. 7 shows that a smaller velocity leads to a greater preheating. Figure 10b shows that leaner flames are, indeed, more preheated. Moreover, these lean flames are more sensitive to an elevation of temperature. Figure 11 presents the impact of temperature variations on the flame speed calculations for adiabatic diluted flames with $p = 5$ atm and $y^0_{H_2O} = 0.3$. The relative increase in flame speed due to temperature increase, written as $[S_l(T_u) - S_l(500\,\text{K})]/S_l(500\,\text{K})$, is plotted for four different equivalence ratios for temperatures between 500 and 700 K. It appears that the leaner a flame is, the more its flame speed is sensitive to an increase in temperature. Thus, leaner flames will be more preheated and more accelerated by an increased temperature which explains the considerable elevation of R for $\phi < 0.5$.

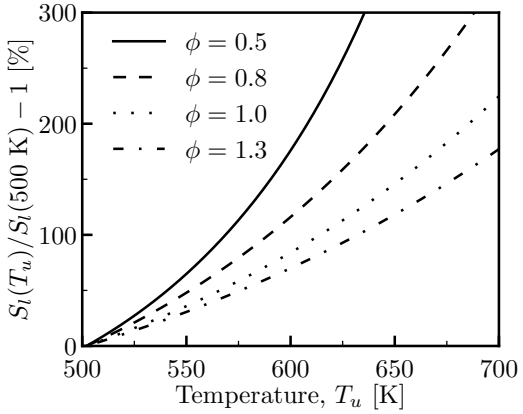

Figure 11: **Temperature sensitivity of adiabatic flame speeds** for different equivalence ratios at $p = 5$ atm, $y^0_{H_2O} = 0.3$ and with $L = 20$ cm.

The R factor reaches remarkable values ($R > 500\%$) for very lean and diluted flames (Figure 10a). However, it should be underlined that these flames have very low adiabatic speeds (~ 2 cm/s) and would be hard to stabilize experimentally and would most likely be blown off. It is nonetheless essential to highlight that the effect of thermal radiation on laminar flame speed is non-negligible for a wide range of equivalence ratios and dilution levels and should be considered in steam-diluted flame simulations.

Figure 12 reproduces Figure 10a but adds in grey the radiative effect estimated from the adiabatic preheated simulation, quantified by a similar R factor written as $(\widehat{S_l}^{\text{rad}} - S_l^{\text{adiab}})/S_l^{\text{adiab}}$, where $\widehat{S_l}^{\text{rad}}$ has been defined in section 4.3. The results are close to those obtained with the coupled radiative simulation for all equivalence ratios and dilution levels. It thus appears that the decoupling of thermal radiation and combustion also applies to most dilution levels and equivalence ratios. When the effect of thermal radiation is the most significant (more than 200%), the temperature gradient just before the flame front is high which makes the definition of the preheating temperature less accurate. In addition, the leanest and most diluted flames are slower and, therefore thicker (for example, at $\phi = 0.7$ and $y^0_{H_2O} = 0.1$, the flame thickness is 70 μm whereas it is 2.4 mm for $y^0_{H_2O} = 0.4$). Thermal radiation will thus tend to interact with the flame itself and, as a result, the decoupling is no longer as good. This explains the differences observed between the radiative and preheated results for high dilution levels and small equivalence ratios.

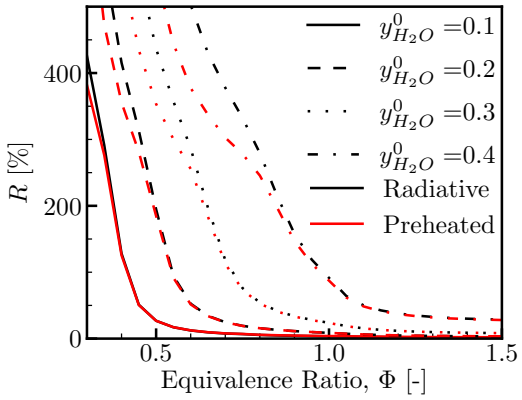

Figure 12: **Comparison of the relative flame speed change R (coupled flame versus estimation from adiabatic preheated flame)** as a function of equivalence ratio for different dilution levels at p = 5 atm and with T_u = 500K and L = 20 cm.

5.3. Pressure

All the simulations presented above were carried out with p = 5 atm. This section studies the impact of pressure change on the coupling between thermal radiation and combustion. As for the equivalence ratio in the previous section, the effect of thermal radiation, quantified by R, is plotted as a function of pressure for $y^0_{H_2O}$ = 0.3 and for different equivalence ratios in Figure 13. At first, it could be thought that increasing the pressure increases the optical thickness of the fresh and burnt gases leading to a stronger thermal radiation effect. It appears that the variations with pressure of R and of the preheating are not that simple as R does not monotonously increase with pressure. These variations can still be explained by considering all the terms in Eq. 7.

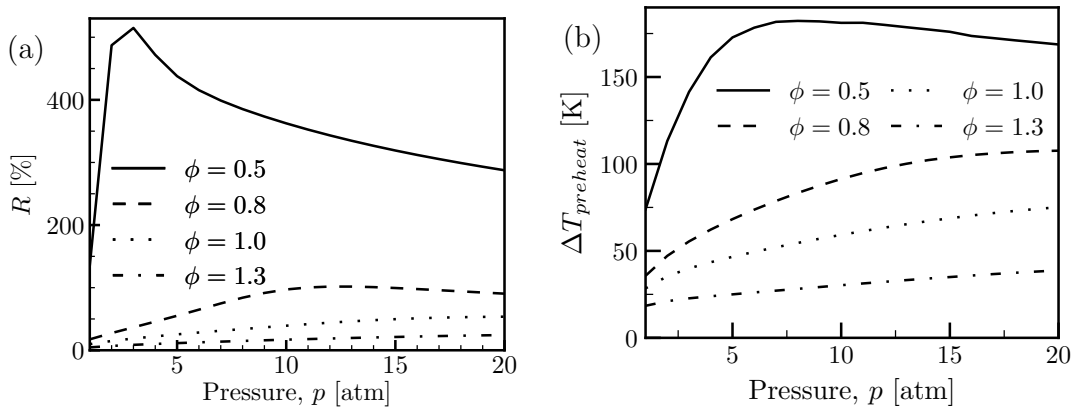

Figure 13: **Impact of pressure on the relative flame speed change** R (a) **and on the preheating** (b) for $y^0_{H_2O}$ = 0.3, T_u = 500K and L = 20 cm. The radiative simulations are carried out with a CK model.

Changing the pressure impacts not only the radiative power but also the density of the mixture as well as the flame speed. It thus affects ρ_u, S_l and Q^{rad} in Eq. 7. For an ideal gas, the variations of the density with pressure are known and $\rho_u \propto p$. To quickly grasp the global effect of pressure on the preheating, it is then interesting to compare the sensitivities of Q^{rad} and S_l to an increase in pressure. Both these sensitivities are illustrated in Figure 14 for different equivalence ratios at $y^0_{H_2O}$ = 0.3. The flame speed sensitivity is obtained with adiabatic simulations while the radiative power sensitivity comes from coupled radiative calculations. The adiabatic flame speed decreases much faster for low pressures at ϕ = 0.5. The integrated radiative power in the fresh gases, Q^{rad}, increases similarly for all equivalence ratios.

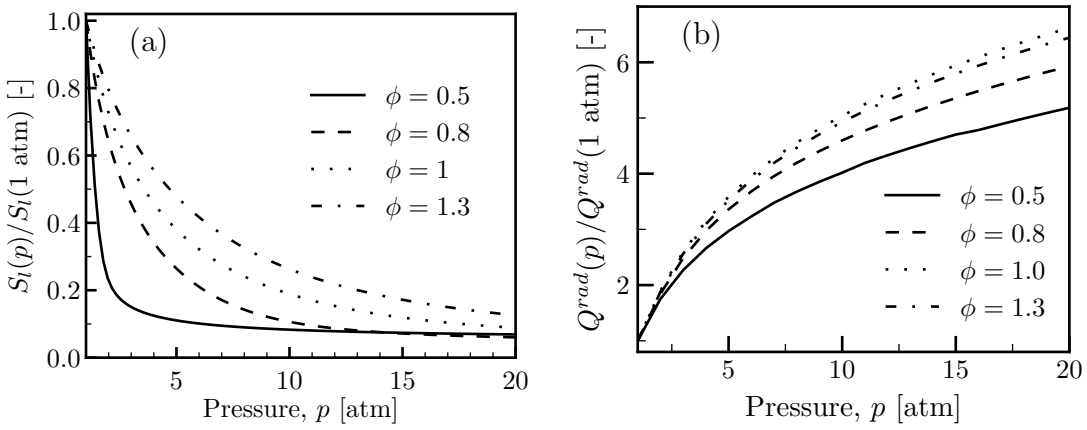

Figure 14: **Relative effect of pressure on the adiabatic flame speed** (a) **and on the integrated radiative power in the fresh mixture,** Q^{rad} (b) for different equivalence ratios at $y^0_{H_2O} = 0.3$ and with $T_u = 500$K and $L = 20$ cm. Results are obtained with adiabatic simulations for (a) and coupled radiative calculations with a CK model for (b).

These sensitivities can be more easily compared thanks to the definition of local coefficients $\alpha_S > 0$ and $\alpha_Q > 0$ such that $S_l \propto p^{-\alpha_S}$ and $Q^{\mathrm{rad}} \propto p^{\alpha_Q}$. Together with the fact that $\rho \propto p$, this leads to:

$$\Delta T_{\mathrm{preheat}} \propto p^{\alpha_S + \alpha_Q - 1} \tag{8}$$

Practically speaking, these coefficients can be obtained by writing

$$\alpha_S = -\frac{d \ln S_l}{d \ln p} \text{ and } \alpha_Q = \frac{d \ln Q^{\mathrm{rad}}}{d \ln p} \tag{9}$$

Figure 15 shows α_S and α_Q for the same four equivalence ratios. For the adiabatic simulations leading to α_S, a hundred flames were computed between 1 and 20 atm leading to $\Delta p = 0.19$ atm. For the coupled radiative simulations leading to α_Q, only integer values of pressure in atm were used to be able to directly apply the radiative property tables of the CK model, *i.e.* $\Delta p = 1$ atm. This larger step explains why the graphs for α_Q are less smooth than that for α_S.

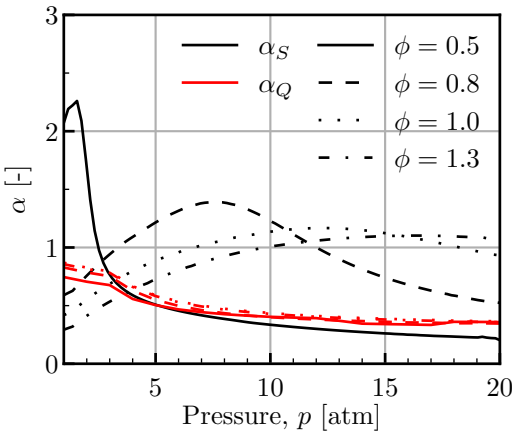

Figure 15: **Pressure variations of sensitivity coefficients** α_Q **and** α_S for different equivalence ratios at $y^0_{H_2O} = 0.3$ and with $T_u = 500$K and $L = 20$ cm. For every pressure, α_Q and α_S are defined such that, around that pressure, $S_l(p) \propto p^{\alpha_S}$ and $Q^{\mathrm{rad}}(p) \propto p^{\alpha_Q}$.

As expected, α_S is the highest for $\phi = 0.5$ and low pressures where the drop in flame speed was observed in Figure 14a. The values of α_Q for the different equivalent ratios are really close to each other which is also coherent with the previous analysis of Figure 14b.

The sum of α_S and α_Q appears to be greater than 1 for all equivalence ratios and pressures except for (i) $\phi = 0.8$ and $p \geq 17$ atm where $\alpha_S + \alpha_Q \lesssim 1$ and for (ii) $\phi = 0.5$ and $p > 5$ atm where $\alpha_S + \alpha_Q < 1$. This means that for most pressures and equivalence ratios, $\alpha_S + \alpha_Q - 1 > 0$ and the radiative preheating increases with pressure. This is in agreement with Figure 13b which shows an increasing preheating with pressure except for $\phi = 0.5$ and high pressures. For $\phi = 0.8$ and $p \geq 17$ atm the preheating reaches a plateau as predicted by $\alpha_S + \alpha_Q \sim 1$.

Thus, the effect of pressure on the radiative preheating can be fully understood by considering not only the increase in optical thickness but also, the impact of pressure on the flame speed and the density of the mixture.

For $\phi = 1$ and $\phi = 1.3$, a greater preheating results directly in a stronger effect of thermal radiation as illustrated in Figure 13a. For the two lean equivalence ratios, the correlation between the preheating and R is not as simple. As in the previous section, the relation between the preheating and the R-factor can be established via the sensitivity of the adiabatic flame speed to a temperature increase. This sensitivity is presented in Figure 16 for $\phi = 0.8$ (Fig. 16a) and $\phi = 0.5$ (Fig. 16b) for four different pressures at $y^0_{H_2O} = 0.3$.

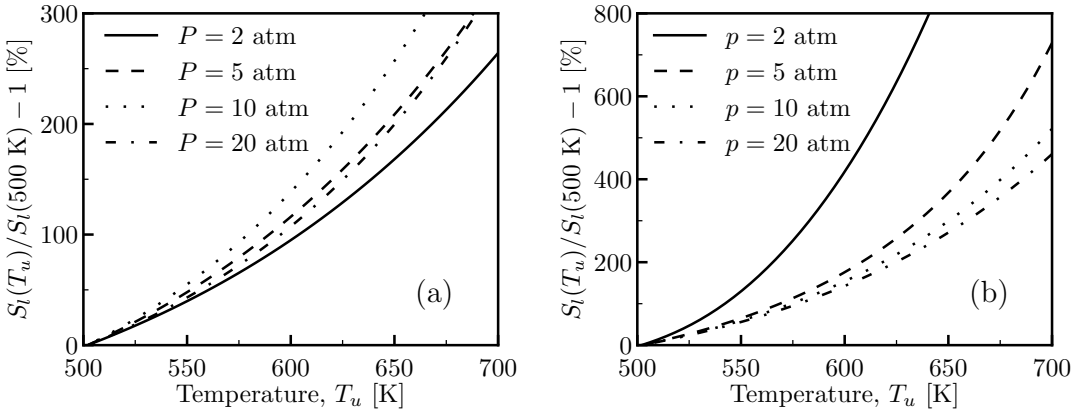

Figure 16: **Relative effect of temperature on the adiabatic flame speed** for $\phi = 0.8$ (a) and $\phi = 0.5$ (b) for different pressures at $y^0_{H_2O} = 0.3$ and with $L = 20$ cm.

For $\phi = 0.8$, the preheating increases considerably between 1 and 2 atm which results in a greater R factor at 2 atm (Figure 13a). The preheating and R factor keep both increasing until around 10 atm. The increase of the preheating between 10 and 20 atm is less significant and becomes not sufficient to compensate for the lower sensitivity to temperature of the 20 atm flame. This explains the slight decrease in R observed in Figure 13a for $\phi = 0.8$ and $p > 10$ atm.

For $\phi = 0.5$, the flame at 2 atm is the most sensitive to temperature changes (Figure 16b). This, combined with a significant preheating (Figure 13b), results in a considerable effect of thermal radiation on this flame ($R \approx 500\%$). The radiative preheating increases a lot between 2 and 10 atm thanks to the steep decrease of the adiabatic flame speed (see Figure 14a). This increase is, though, insufficient to compensate for the lower temperature sensitivities of the 5 and 10 atm flames, and R decreases between 3 and 10 atm. Finally, between 10 and 20 atm the preheating gets smaller and smaller (Figure 13b) and the flame is ever less sensitive to temperature (Figure 16b). The combination of both these effects leads to a significant decrease of R between 10 and 20 atm (Figure 13a).

The effect of pressure on the coupling of thermal radiation and combustion has been detailed and explained. It was found that the acceleration of diluted flames by radiation is consequent for a wide range of pressures. As in the previous section, it is noteworthy that the lean flames at $\phi = 0.5$ and $p \geq 2$ atm have very small adiabatic flame speeds (< 2 cm/s).

Finally, Figure 17 reproduces Figure 13a but adds in grey the radiative R factor estimated with the adiabatic preheated flame. The decoupling of the preheating and combustion also applies to most pressures. As seen in section

5.2, the decoupling is not as complete for leaner flames ($\phi = 0.5$) where the effect of thermal radiation is the most significant.

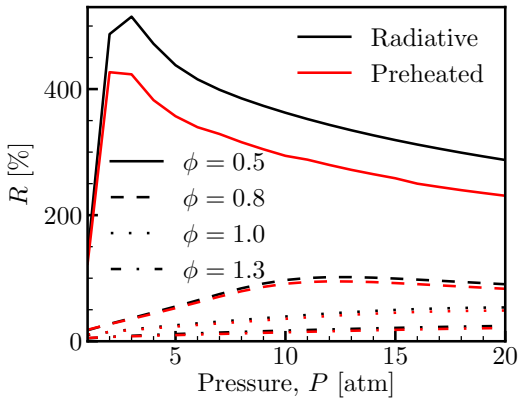

Figure 17: **Comparison of the relative flame speed change R (coupled flame versus estimation from adiabatic preheated flame)** as a function of pressure for different equivalence ratios at $y^0_{H_2O} = 0.3$ atm and with $T_u = 500$K and $L = 20$ cm.

6. Conclusions

This study has investigated the effect of thermal radiation on premixed 1D H_2-Air flames diluted with steam using a reactive fluid solver coupled with a semi-analytical solution for thermal radiation. Initially, a grey gas approximation has been used to obtain preliminary insights on the coupling between thermal radiation and combustion. However, for the detailed simulations, an accurate spectral-dependent CK model is chosen instead. The results have shown that radiative heat transfer significantly impacts flame characteristics, including a preheating of the fresh gases, an increase in the laminar flame speed, and a decrease in temperature in the burnt gases. For a specific flame with realistic conditions, it was shown that the consideration of thermal radiation increases the flame speed by more than 50%.

Since the characteristic scales of thermal radiation are much bigger than those of combustion, it was shown that the two phenomena can often be decoupled. Adiabatic preheated flames, with a fresh mixture temperature equal to the preheating temperature of the corresponding coupled radiative flames, can recover most of the coupled flame characteristics such as its maximum temperature or its burning mass flow rate. This decoupled regime is similar to the one observed with porous burners by Masset *et al.* [49]. More entangled coupled regimes were underlined in [49] and it would be interesting, in future work, to see if these other regimes (intermediate or even hyper-diffusive) also exist for the coupling between thermal radiation and gaseous-phase combustion.

The effect of thermal radiation on the laminar flame speed was quantified and explained for a wide range of pressures, equivalence ratios and dilution levels. It was found that lean, diluted flames are the most impacted with an increase in flame speed as big as 500% for very slow flames. Even for faster flames with $S_l \sim 20$ cm/s, the acceleration can exceed 50% with $y^0_{H_2O} \geq 20\%$. The impact of domain length on the flame acceleration due to thermal radiation has also been examined, highlighting the importance of considering this parameter in combustion simulations.

Overall, this study emphasizes the necessity of considering thermal radiation in 1D simulations of steam-diluted flames to achieve accurate predictions of flame characteristics, such as its unstretched laminar flame speed, a fundamental property in combustion modeling and 3D practical applications.

Future studies should focus on 3D coupled laminar or turbulent flame computations that could be more easily compared to experimental results. For lean hydrogen flames, where the thermal radiation effect is the most significant, it would also be interesting to see how thermal radiation interacts with thermo-diffusive instabilities.

Acknowledgements

This work was performed using HPC resources from the "Mésocentre" computing center of CentraleSupélec, École Normale Supérieure Paris-Saclay and Université Paris-Saclay supported by CNRS and Région Île-de-France (https://mesocentre.universite-paris-scalay.fr/) and from GENCI–IDRIS (Grant 2022-TMP21060).

The authors also acknowledge Dr. Philippe Rivière for providing the CK model database.

References

[1] R. Grosseuvres, A. Comandini, A. Bentaib, N. Chaumeix, Combustion properties of H2/N2/O2/steam mixtures, Proc. Combust. Inst. 37 (2019) 1537–1546.
[2] D. Liu, R. MacFarlane, Laminar burning velocities of hydrogen-air and hydrogen-air steam flames, Combust. Flame 49 (1983) 59–71.
[3] G. Koroll, S. Mulpuru, The effect of dilution with steam on the burning velocity and structure of premixed hydrogen flames, Symp. (Int.) Combust. 21 (1988) 1811–1819.
[4] A. K. Das, K. Kumar, C.-J. Sung, Laminar flame speeds of moist syngas mixtures, Combust. Flame 158 (2011) 345–353.
[5] Y. Xie, J. Wang, N. Xu, S. Yu, Z. Huang, Comparative study on the effect of CO2 and H2O dilution on laminar burning characteristics of CO/H2/air mixtures, Int. J. Hydrogen Energ. 39 (2014) 3450–3458.
[6] S. Meng, S. Sun, H. Xu, Y. Guo, D. Feng, Y. Zhao, P. Wang, Y. Qin, The effects of water addition on the laminar flame speeds of CO/H2/O2/H2O mixtures, Int. J. Hydrogen Energ. 41 (2016) 10976–10985.
[7] Y. Lyu, P. Qiu, L. Liu, C. Yang, S. Sun, Effects of steam dilution on laminar flame speeds of H2/air/H2O mixtures at atmospheric and elevated pressures, Int. J. Hydrogen Energ. 43 (2018) 7538–7549.
[8] Y. Lyu, A. Aspden, L. Zhang, L. Liu, P. Qiu, Study of the chemical effect of steam dilution on NO formation in laminar premixed H2/Air flame at normal and elevated pressure, Int. J. Hydrogen Energ. 46 (2021) 13402–13412.
[9] C. H. Sohn, Z. Chen, Y. Ju, Effects of radiation on the uncertainty of flame speed determination using spherically propagating flames with CO/CO2/H2O dilutions at elevated pressures, Int. J. Heat Mass Tran. 86 (2015) 820–825.
[10] Z. Chen, X. Qin, B. Xu, Y. Ju, F. Liu, Studies of radiation absorption on flame speed and flammability limit of CO2 diluted methane flames at elevated pressures, Proc. Combust. Inst. 31 (2007) 2693–2700.
[11] M. Han, Y. Ai, Z. Chen, W. Kong, Laminar flame speeds of H 2 /CO with CO 2 dilution at normal and elevated pressures and temperatures, Fuel 148 (2015) 32–38.
[12] Z. Chen, Effects of radiation absorption on spherical flame propagation and radiation-induced uncertainty in laminar flame speed measurement, Proc. Combust. Inst. 36 (2017) 1129–1136.
[13] Z. Chen, Effects of radiation on large-scale spherical flame propagation, Combust. Flame 183 (2017) 66–74.
[14] Y. Ju, G. Masuya, P. D. Ronney, Effects of radiative emission and absorption on the propagation and extinction of premixed gas flames, Symp. (Int.) Combust. 27 (1998) 2619–2626.
[15] J. Ruan, H. Kobayashi, T. Niioka, Y. Ju, Combined effects of nongray radiation and pressure on premixed CH4/O2/CO2 flames, Combust. Flame 124 (2001) 225–230.
[16] S. Zheng, H. Liu, R. Sui, B. Zhou, Q. Lu, Effects of radiation reabsorption on laminar NH3/H2/air flames, Combustion and Flame 235 (2022) 111699.
[17] S. Zheng, H. Liu, D. Li, Z. Liu, B. Zhou, Q. Lu, Effects of radiation reabsorption on the laminar burning velocity of methane/air and methane/hydrogen/air flames at elevated pressures, Fuel 311 (2022) 122586.
[18] S. Zheng, H. Liu, Y. He, Y. Yang, R. Sui, Q. Lu, Combustion of biomass pyrolysis gas: Roles of radiation reabsorption and water content, Renewable Energy 205 (2023) 864–872.
[19] T. Varga, T. Nagy, C. Olm, I.Gy. Zsély, R. Pálvölgyi, É. Valkó, G. Vincze, M. Cserháti, H. Curran, T. Turányi, Optimization of a hydrogen combustion mechanism using both direct and indirect measurements, Proc. Combust. Inst. 35 (2015) 589–596.
[20] A. L. Sánchez, F. A. Williams, Recent advances in understanding of flammability characteristics of hydrogen, Prog. Energ. Combust. 41 (2014) 1–55.
[21] M. F. Modest, Radiative Heat Transfer, McGraw-Hill Series in Mechanical Engineering, McGraw-Hill, New York, 1993.
[22] R. Goody, R. West, L. Chen, D. Crisp, The correlated-k method for radiation calculations in nonhomogeneous atmospheres, J. Quant. Spectrosc. Ra 42 (1989) 539–550.
[23] P. Rivière, A. Soufiani, Updated band model parameters for H2O, CO2, CH4 and CO radiation at high temperature, Int. J. Heat Mass Tran. 55 (2012) 3349–3358.
[24] J. Taine, A. Soufiani, Gas IR Radiative Properties: From Spectroscopic Data to Approximate Models, in: J. P. Hartnett, T. F. Irvine, Y. I. Cho, G. A. Greene (Eds.), Advances in Heat Transfer, Vol. 33, Elsevier, 1999, pp. 295–414.
[25] C. Xiouris, T. Ye, J. Jayachandran, F. N. Egolfopoulos, Laminar flame speeds under engine-relevant conditions: Uncertainty quantification and minimization in spherically expanding flame experiments, Combust. Flame 163 (2016) 270–283.
[26] A. Bhargava, M. Colket, W. Sowa, K. Casleton, D. Maloney, An Experimental and Modeling Study of Humid Air Premixed Flames, J. Eng. Gas Turb. Power 122 (2000) 405–411.
[27] O. Krüger, S. Terhaar, C. O. Paschereit, C. Duwig, Large Eddy Simulations of Hydrogen Oxidation at Ultra-Wet Conditions in a Model Gas Turbine Combustor Applying Detailed Chemistry, J. Eng. Gas Turb. Power 135 (2013) 021501.
[28] R. Xue, C. Hu, V. Sethi, T. Nikolaidis, P. Pilidis, Effect of steam addition on gas turbine combustor design and performance, Appl. Therm. Eng. 104 (2016) 249–257.

[29] C. P. Mark, A. Selwyn, Design and analysis of annular combustion chamber of a low bypass turbofan engine in a jet trainer aircraft, Propuls. Power Res. 5 (2016) 97–107.
[30] R. J. Kee, J. F. Grcar, M. D. Smooke, J. A. Miller, E. Meeks, PREMIX: A FORTRAN Program for Modeling Steady Laminar One-Dimensional Premixed Flames, 1985.
[31] M. P. Burke, Z. Chen, Y. Ju, F. L. Dryer, Effect of cylindrical confinement on the determination of laminar flame speeds using outwardly propagating flames, Combust. Flame 156 (2009) 771–779.
[32] A. Dahoe, Laminar burning velocities of hydrogen–air mixtures from closed vessel gas explosions, J. Loss Prevent Proc. Ind. 18 (2005) 152–166.
[33] G. Dayma, F. Halter, P. Dagaut, New insights into the peculiar behavior of laminar burning velocities of hydrogen–air flames according to pressure and equivalence ratio, Combust. Flame 161 (2014) 2235–2241.
[34] D. R. Dowdy, D. B. Smith, S. C. Taylor, A. Williams, The use of expanding spherical flames to determine burning velocities and stretch effects in hydrogen/air mixtures, Symp. (Int.) Combust. 23 (1991) 325–332.
[35] F. N. Egolfopoulos, C. K. Law, An experimental and computational study of the burning rates of ultra-lean to moderately-rich H2/O2/N2 laminar flames with pressure variation, Symp. (Int.) Combust. (1990) 333–340.
[36] Z. Huang, Y. Zhang, K. Zeng, B. Liu, Q. Wang, D. Jiang, Measurements of laminar burning velocities for natural gas–hydrogen–air mixtures, Combust. Flame 146 (2006) 302–311.
[37] M. C. Krejci, O. Mathieu, A. J. Vissotski, S. Ravi, T. G. Sikes, E. L. Petersen, A. Kérmonès, W. Metcalfe, H. J. Curran, Laminar Flame Speed and Ignition Delay Time Data for the Kinetic Modeling of Hydrogen and Syngas Fuel Blends, J. Eng. Gas Turb. Power 135 (2013) 021503.
[38] M. Kuznetsov, S. Kobelt, J. Grune, T. Jordan, Flammability limits and laminar flame speed of hydrogen–air mixtures at sub-atmospheric pressures, Int. J. Hydrogen Energ. 37 (2012) 17580–17588.
[39] O. Kwon, G. Faeth, Flame/stretch interactions of premixed hydrogen-fueled flames: Measurements and predictions, Combust. Flame 124 (2001) 590–610.
[40] N. Lamoureux, N. Djeba, Laminar flame velocity determination for H2–air–He–CO2 mixtures using the spherical bomb method, Exp. Therm. Fluid Sci. (2003) 385–393.
[41] S. Tse, D. Zhu, C. Law, Morphology and burning rates of expanding spherical flames in H2/O2/inert mixtures up to 60 atmospheres, Proc. Combust. Inst. 28 (2000) 1793–1800.
[42] C. Vagelopoulos, F. Egolfopoulos, C. Law, Further considerations on the determination of laminar flame speeds with the counterflow twin-flame technique, Symp. (Int.) Combust. 25 (1994) 1341–1347.
[43] K. T. Aung, G. M. Faeth, Effects of Pressure and Nitrogen Dilution on Flame/Stretch Interactions of Laminar Premixed H 2/O2/N2 Flames, Combust. Flame (1998) 1–15.
[44] J. Pareja, H. J. Burbano, Y. Ogami, Measurements of the laminar burning velocity of hydrogen–air premixed flames, Int. J. Hydrogen Energ. 35 (2010) 1812–1818.
[45] E. Hu, Z. Huang, J. He, H. Miao, Experimental and numerical study on laminar burning velocities and flame instabilities of hydrogen–air mixtures at elevated pressures and temperatures, Int. J. Hydrogen Energ. 34 (2009) 8741–8755.
[46] M. Kuznetsov, M. Czerniak, J. Grüne, T. Jordan, Effect of temperature on laminar flame velocity for hydrogen-air mixtures at reduced pressures, International Conference on Hydrogen Safety (2013) paper 231.
[47] A. A. Konnov, A. Mohammad, V. R. Kishore, N. I. Kim, C. Prathap, S. Kumar, A comprehensive review of measurements and data analysis of laminar burning velocities for various fuel+air mixtures, Prog. Energ. Combust. 68 (2018) 197–267.
[48] N. Lamoureux, N. Chaumeix, C. Paillard, Laminar flame velocity determination for H2-air-steam mixtures using the spherical bomb method, J. Phys. IV (2002) 445–452.
[49] P. A. Masset, O. Dounia, L. Selle, Combustion regimes in inert porous media: From decoupled to hyperdiffusive flames, Combust. Flame 241 (2022) 112052.
[50] H. C. Hottel, A. F. Sarofim, Radiative Transport, Mc Cravy Hill (1965) –.
[51] M. F. Modest, The Weighted-Sum-of-Gray-Gases Model for Arbitrary Solution Methods in Radiative Transfer, Journal of Heat Transfer 113 (3) (1991).
[52] M. K. Denison, B. W. Webb, A Spectral Line-Based Weighted-Sum-of-Gray-Gases Model for Arbitrary RTE Solvers, Journal of Heat Transfer 115 (4) (1993) 1004–1012.
[53] Q. Binauld, P. Rivière, A. Soufiani, A note on radiation preheating of some hydrocarbons by combustion products, Combust. Flame 194 (2018) 128–134.
[54] Z. Chen, On the accuracy of laminar flame speeds measured from outwardly propagating spherical flames: Methane/air at normal temperature and pressure, Combust. Flame 162 (2015) 2442–2453.
[55] H. Yu, W. Han, J. Santner, X. Gou, C. H. Sohn, Y. Ju, Z. Chen, Radiation-induced uncertainty in laminar flame speed measured from propagating spherical flames, Combust. Flame 161 (2014) 2815–2824.

Supplemental Material for

Acceleration of premixed H_2-Air-Steam Flames when accounting for thermal radiation

J. Ben Zenou[1*] R. Vicquelin[1]

[1]Universite Paris-Saclay, CNRS, CentraleSupelec, Laboratoire EM2C

A. Comparison of the results from the combustion and radiation solver with other numerical results

A.1. Mesh convergence

A comparison of the results obtained with the Agath code and with the Chemkin Premix code [1] are presented here for the condition detailed in the manuscript ($p = 5$ atm, $T_u = 500$ K, $\phi = 0.8$ and $y^0_{H_2O} = 0.3$) in the adiabatic case. As in the manuscript, the Varga mechanism [2] is used for hydrogen combustion. The solutions presented here are independent on the mesh size and correspond to the last point seen in Figure S.1 for each line.

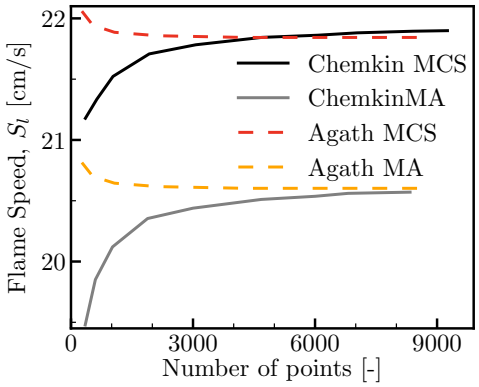

Figure S.1: Mesh convergence of the laminar flame speed using Agath (dashed lines) or Chemkin (full lines) and the MultiComponent formulation with the Soret effect (MCS, black or red) or the Mixture averaged formulation without the Soret effect (MA, grey or orange).

The solutions presented in the manuscript were not obtained with a mesh as fine as the one used for this validation to improve the speed of the simulations. The criteria retained for the mesh is a 4% maximum change in the relative variation of the solution fields (parameter GRAD in Chemkin) and of the derivative of the solution fields (parameter CURV in Chemkin). For the condition detailed in the manuscript ($p = 5$ atm, $T_u = 500$ K, $\phi = 0.8$ and $y^0_{H_2O} = 0.3$), the adiabatic flame speed is $S_l = 22.04$ cm/s which corresponds to a 0.9% difference with the most refined solution obtained with Agath. This confirms that the results presented in the manuscript can be considered grid-independent.

A.2. Comparison of the results from Agath with those from Chemkin PREMIX

The temperature profiles obtained with Agath and Chemkin are compared in Figure S.2 for both the mixture averaged transport description and the multicomponent formulation considering the Soret effect. In order to validate the flame structure, the temperature, the heat release rate, y_{OH}, y_H, and y_{H_2} are also plotted as a function of y_{H_2O} in Figure S.3. The plots show an almost perfect overlap between the results from both codes and confirm the importance of an accurate transport description. With the multicomponent formulation and the soret effect, the laminar flame speed obtained with Chemkin is 21.88 cm/s which can be compared with the 21.84 cm/s obtained with Agath in the adiabatic case. This corresponds to less than a 0.2% difference. This validates the 1D combustion solver used in the manuscript.

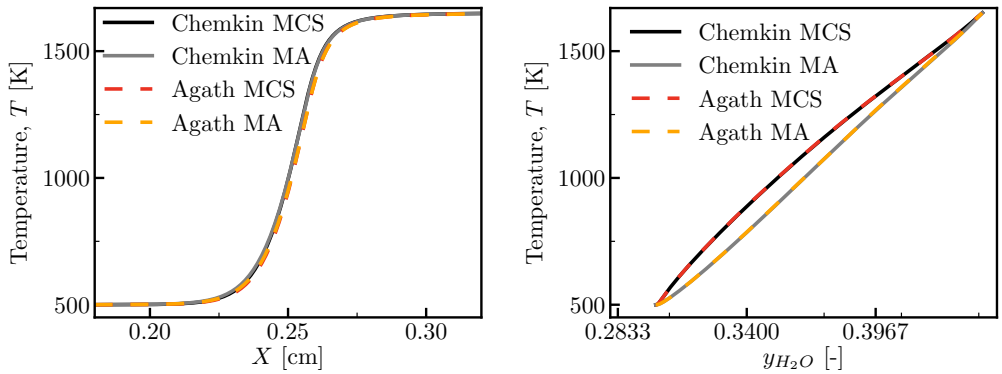

Figure S.2: Comparison of the adiabatic temperature profiles (as a function of position on the left and y_{H_2O} on the right) obtained with Agath (dashed lines) or Chemkin (full lines) and the MultiComponent formulation with the Soret effect (MCS, black or red) or the Mixture averaged formulation without the Soret effect (MA, grey or orange). $p = 5$ atm, $T_u = 500$ K, $\phi = 0.8$ and $y^0_{H_2O} = 0.3$.

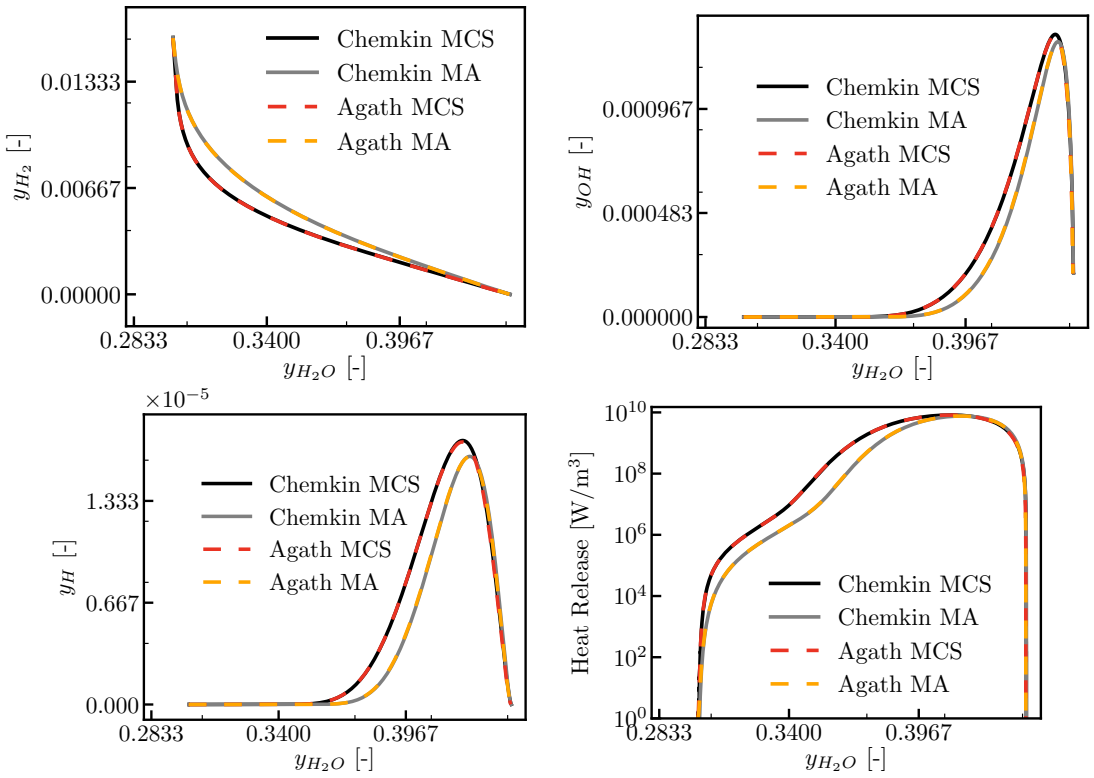

Figure S.3: y_{H_2}, y_{OH}, y_H and Heat Release Rate as a function of y_{H_2O} obtained with Agath (dashed lines) or Chemkin (full lines) and the MultiComponent formulation with the Soret effect (MCS, black or red) or the Mixture averaged formulation without the Soret effect (MA, grey or orange). $p = 5$ atm, $T_u = 500$ K, $\phi = 0.8$ and $y^0_{H_2O} = 0.3$.

A.3. Comparison of the results from the 1D radiative solver and the CK model with those from the literature

First, previous calculations of column emissivities with the same CK parameters [3] have shown very good agreement when compared to line-by-line results.

Second, the results of the 1D solver with a Grey Gas model are compared to those by Tessé et al. [4]. The reference results for their "Case 1" with $\kappa L = 2$, $L = 0.2$ m, a total pressure of 1 atm, a wall emissivity of $\varepsilon_w = 0.8$, a wall temperature of $T_w = 500$ K and a gas temperature following a parabolic profile with a maximum of $T_{c_s} = 2500$ K are reproduced in Figure S.4. The results from the 1D solver used in the manuscript appear to be really close to those from the original paper [4] with a maximum relative difference of 2.5% mostly due to the uncertainty on the digitalization of the reference results. This validates the implementation of the 1D semi-analytical solution with a grey gas.

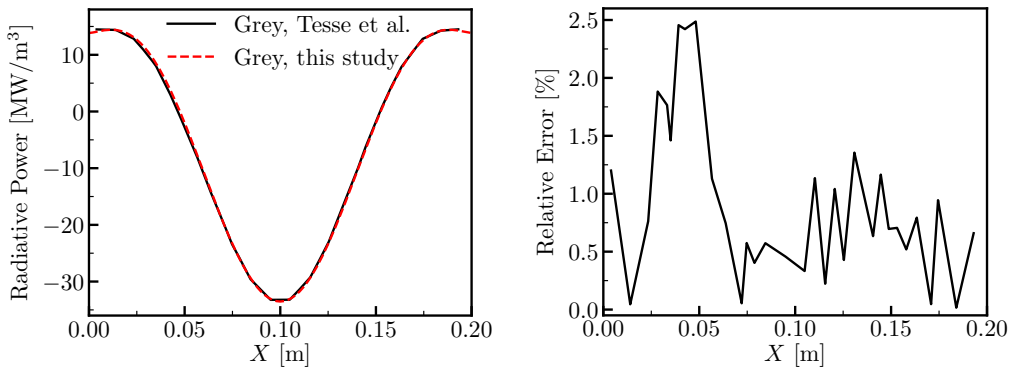

Figure S.4: Comparison of the radiative power obtained in a 0.2m 1D slab with a grey model ($\kappa L = 2$) by [4] and by the 1D solver used in the manuscript.

Finally, the results of the 1D solver with the CK model are compared to those found in [5]. In this study, Chu and co-workers solve the radiative transfer equation in 1D slabs with a Discrete Ordinate Method (DOM) and both an LBL and an SNB model. The temperature is constant with $T = 1000$ K and only H_2O is present in the slab with $x_{H_2O} = 1.0$. The total pressure is 1 atm. The walls are considered black and at 300 K and the slab length is 0.1 m. The radiative power profiles obtained with the LBL model, the SNB model and the 1D solver used in the manuscript with the CK model from [6] are plotted in Figure S.5. The results obtained with the CK model overlap perfectly with those obtained with an LBL model in [5] (maximum relative difference of 1.5%, once again, mostly due to the uncertainty on the digitalization of the reference results). This validates the use of the 1D radiative solver with the CK model.

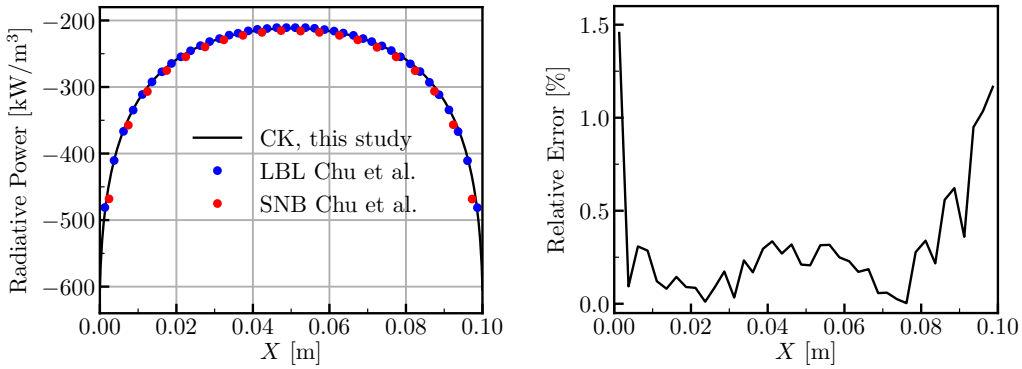

Figure S.5: Comparison of the radiative power obtained in a 1m 1D slab with the LBL and SNB models used in [5] as well as with the 1D solver used in the manuscript and the CK model from [6].

References

[1] R. J. Kee, J. F. Grcar, M. D. Smooke, J. A. Miller, E. Meeks, PREMIX: A FORTRAN Program for Modeling Steady Laminar One-Dimensional Premixed Flames, 1985.

*Corresponding author: julie.benzenou@centralesupelec.fr

[2] T. Varga, T. Nagy, C. Olm, I.Gy. Zsély, R. Pálvölgyi, É. Valkó, G. Vincze, M. Cserháti, H. Curran, T. Turányi, Optimization of a hydrogen combustion mechanism using both direct and indirect measurements, Proc. Combust. Inst. 35 (2015) 589–596.

[3] J. M. Armengol, R. Vicquelin, A. Coussement, R. G. Santos, O. Gicquel, Study of turbulence-radiation interactions in a heated jet using direct numerical simulation coupled to a non-gray Monte-Carlo solver, International Journal of Heat and Mass Transfer 162 (2020) 120297.

[4] L. Tessé, F. Dupoirieux, B. Zamuner, J. Taine, Radiative transfer in real gases using reciprocal and forward Monte Carlo methods and a correlated-k approach, Int. J. Heat Mass Tran. 45 (13) (2002) 2797–2814.

[5] H. Chu, F. Liu, H. Zhou, Calculations of gas thermal radiation transfer in one-dimensional planar enclosure using LBL and SNB models, International Journal of Heat and Mass Transfer 54 (21) (2011) 4736–4745.

[6] P. Rivière, A. Soufiani, Updated band model parameters for H2O, CO2, CH4 and CO radiation at high temperature, Int. J. Heat Mass Tran. 55 (2012) 3349–3358.